

Cooling-Rate Effects in Sodium Silicate Glasses: Bridging the Gap between Molecular Dynamics Simulations and Experiments

Xin Li¹, Weiying Song¹, Kai Yang¹, N M Anoop Krishnan¹, Bu Wang¹, Gaurav Sant², Mathieu Bauchy^{1*}

¹Physics of Amorphous and Inorganic Solids Laboratory (PARISlab), 5731B Boelter Hall, University of California, Los Angeles, CA 90095-1593, U.S.A.

²Laboratory for the Chemistry of Construction Materials, 2517 Boelter Hall, University of California, Los Angeles, CA 90095-1593, U.S.A.

*Corresponding author: Prof. Mathieu Bauchy, bauchy@ucla.edu

Abstract

Although molecular dynamics (MD) are commonly used to predict the structure and properties of glasses, they are intrinsically limited to high cooling rates. Our lack of knowledge regarding the effects of the cooling rate on glasses' properties therefore render challenging meaningful comparisons between simulated and experimental results. Here, based on MD simulations of a sodium silicate glass with varying cooling rates, we show that the thermal history mostly affects the medium-range order structure, while leaving the short-range order largely unaffected. This yields a decoupling between the relaxations of the enthalpy and volume, namely, the enthalpy quickly plateaus as the cooling rate decreases whereas density exhibits a slower relaxation. Finally, we demonstrate that the outcomes of MD simulations can be meaningfully compared to experimental values if properly extrapolated toward lower cooling rates.

I. Introduction

Molecular dynamics simulations are now commonly used to investigate the structure and dynamics of disordered atomic networks [1–4], which often remains “invisible” to traditional experiments, despite recent advances [5]. However, the structural characterization of disordered networks is complicated by the fact that glasses are out-of-equilibrium and continually relax toward the metastable supercooled liquid equilibrium state [6]. As such, the structure and property of glasses depend on their thermal history, e.g., the cooling rate during quenching [4]. This raises serious questions regarding the reliability of MD simulations since the cooling rate used in such simulations is typically on the order of 10^{12} K/s, that is, much higher than that typically achieved experimentally (1-to-100 K/s).

Several studies have investigated the effect of the cooling rate of the structure and properties of model glasses [7] and silica [4,8,9], among others. In silica, it is typically observed that the usage of high cooling rates results in the formation of unrealistic structural defects [9], although the overall structure only weakly depends on the thermal history [4]. In contrast, some properties, e.g., the density or thermal expansion, were found to be highly sensitive to the cooling rate [8]. However, silica features various unique properties, including (1) a high connectivity, which prevents any structural relaxation at low temperature [10], (2) a low fragility index [11], which limits the propensity for relaxation within the supercooled liquid state close to the glass transition temperature (T_g), and (3) an anomalous V–T diagram at high temperature [6]. Since all these features can affect the relaxation of the system upon cooling, it remains unclear whether the cooling-rate-dependence of the structure and properties of silica is representative of that of more depolymerized and fragile silicate glasses that industrially relevant. More generally, this raises the following questions: Are MD simulations representative of real glasses? Can their outcomes be reliably extrapolated to the low cooling rate typically used experimentally?

To partially answer these questions, we rely here on MD simulations of a sodium silicate glass, (an archetypical model for various multi-components silicate glasses of industrial [12–15] and geological [16] relevance) prepared under various cooling rates, ranging from 100 to 0.01 K/ps. We show that, although the short-range order structure remains largely unaffected by the cooling rate, medium-range order structural features like the Q^n distribution exhibit a stronger dependence on the cooling rate. These distinct behaviors are found to yield a decoupling between the relaxation of the enthalpy and volume upon decreasing cooling rate. Finally, we demonstrate that, although they are limited to high cooling rates, MD simulations offer predictions that can be quantitatively compared to experimental values, provided that they are properly extrapolated toward lower cooling rates.

II. Simulations details

1. Preparation of the glasses

To establish our conclusions, we rely here on a sodium silicate glass $(\text{Na}_2\text{O})_{30}(\text{SiO}_2)_{70}$ comprising 3000 atoms. The system was simulated via the classical MD approach, using the well-established Teter potential [17–19]. Following previous studies, a short-range repulsion term was added to avoid the “Buckingham catastrophe” at high temperature [1,19]. Cutoffs of 8 and 12 Å were used for the short-range and Coulombic interactions, respectively. The Coulombic interactions were evaluated with the PPPM algorithm with an accuracy of 10^{-5} . All simulations were run using the LAMMPS package [20] with a fixed timestep of 1.0 fs.

The glasses were simulated using the traditional melt-quench procedure as follows. First, the atoms were randomly placed within a cubic box while ensuring the absence of any unrealistic overlap. The system was then melted at 4000 K in the canonical (NVT) ensemble for 10 ps and under zero pressure (NPT ensemble) for 100 ps, which ensuring the complete loss of the memory of the initial configuration. The system was subsequently linearly cooled to 300 K under zero pressure (NPT ensemble) with five cooling rates covering four orders of magnitude: 100 K/ps, 10

K/ps, 1 K/ps, 0.1 K/ps, and 0.01 K/ps. Note that this represent a significant computational effort as most MD simulations typically rely on cooling rates equal or larger than 1 K/ps. All the formed glasses were further relaxed at 300 K and zero pressure for 100 ps before a *NVT* run of 100 ps for statistical averaging. In the following, all properties referring to the “glassy state” were averaged over 100 configurations extracted from this run.

2. Glass transition and inherent configurations

To carefully track when the system falls out-of-equilibrium, that is, the glass transition, we computed the enthalpy of the inherent configurations (noted ground-state enthalpy in the following) explored by the system as a function of temperature. This was achieved as follows. First, for each cooling rate, 16 independent configurations were *a posteriori* extracted during the cooling rate every 100 K. Each configuration was then subjected to an energy minimization. The ground state enthalpy was subsequently calculated by averaging the final enthalpies of the 16 relaxed configurations. Finally, for each cooling rate, the fictive temperature (T_f , see Sec. III.1) was determined by the linearly fitting the low- and high-temperature domains of the ground-state enthalpy and determining the temperature at which these lines intercept.

3. Accuracy of the potential

The ability of the Teter potential to predict the features of sodium silicate glasses has already extensively been discussed [17–19,21,22]. In particular, it has been shows to yield realistic structural [17,23], dynamical [16,24,25], vibrational [19], thermodynamical [19,26,27], and mechanical [28–31] properties. To illustrate these features, Fig. 1 shows the neutron pair distribution function and structure factor [19] computed for the glass prepared with a cooling rate of 0.01 K/ps, which are compared to neutron diffraction data [32]. Note that the pair distribution function was broadened to account for the maximum of wave vector ($Q_{\max} = 22.88 \text{ \AA}^{-1}$) used experimentally [33]. This was achieved by convoluting the computed neutron pair distribution function with a normalized Gaussian distribution with a full width at half-maximum (FWHM) given by $\text{FWHM} = 5.437/Q_{\max}$ [33]. As shown in Fig. 1, both the neutron pair distribution function and structure factor show a very good agreement with the experimental data.

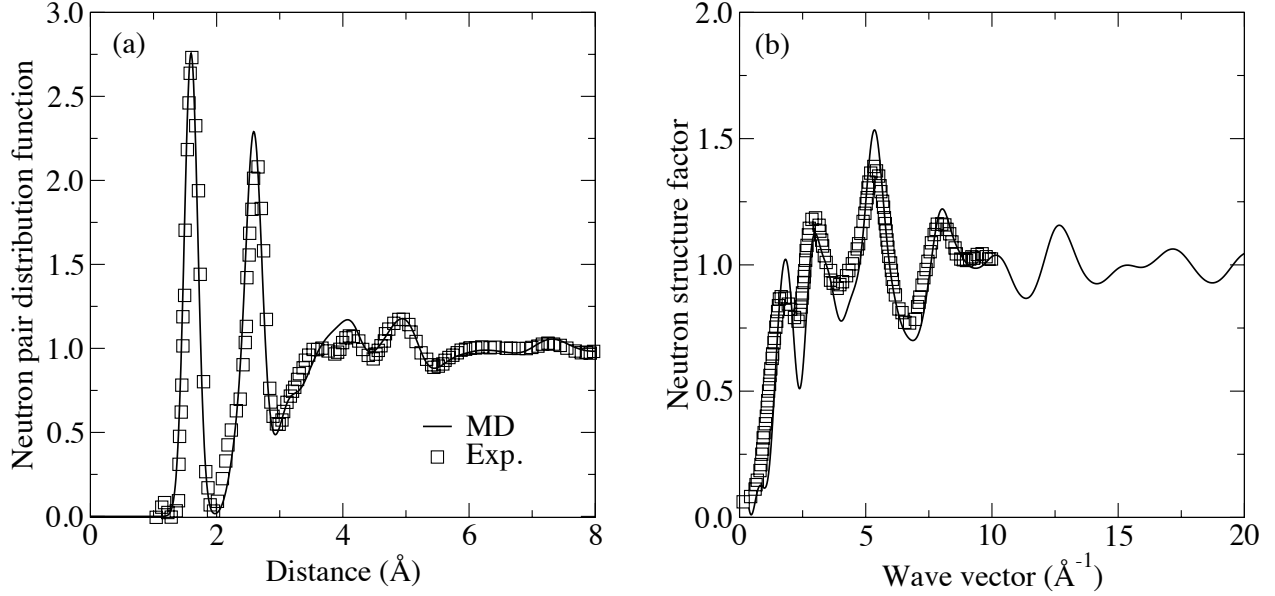


Fig. 1: Computed (a) neutron pair distribution function and (b) structure factor in the glassy state. The results are compared to neutron diffraction data [32].

III. Results

1. Glass transition

We first focus on the temperature-dependence of the ground-state enthalpy (see Sec. II.2) to ensure that our methodology yields realistic results regarding the influence of the cooling rate. As shown in Fig. 2, we observe that the ground-state enthalpy decreases monotonically with decreasing temperature. At a given temperature, a break of slope is observed, which indicates that the system falls out-of-equilibrium. This corresponds to the point at which the relaxation time of the system starts to exceed the observation time, that is, to the supercooled-liquid-to-glassy transition. In the following, we refer to this temperature as the “fictive temperature” of the glass as the “glass transition temperature” (T_g) is traditionally defined as the temperature at which the viscosity of the glass reaches 10^{12} Pa·s [6], which cannot be directly assessed by conventional MD simulations. Note that, in contrast to glassy silica, the ground-state enthalpy of sodium silica continues to decrease in the glassy state (low temperature), which indicates that, in agreement with recent experiments and simulations [34,35], some extent of structural relaxation continues to occur below the glass transition temperature.

Further, we observe that our simulations reproduce the typical features of the glass transition that are observed experimentally [6]. Namely, the usage of slower cooling rate result in (1) lower values of fictive temperatures (see Fig. 12 in Sec. IV.1) and (2) lower values of the final ground-state enthalpy in the glassy state (see the inset of Fig. 2). As expected, this indicates that (1) the system can remain in the metastable equilibrium supercooled liquid state until lower temperatures as the cooling rate decreases, i.e., as the observation time increases, and (2) the glass can achieve a more stable (lower ground-state enthalpy) configuration as the cooling rate decreases, as it has more time to efficiently sample the enthalpy landscape [36]. Note that the

difference of ground-state enthalpy between the glasses obtained using the highest and lowest cooling rates is on the order of 40 meV/atom.

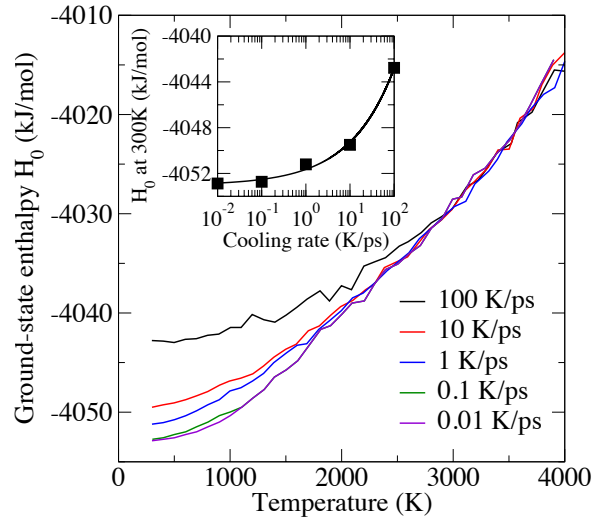


Fig. 2: Ground-state enthalpy (H_0) as a function of temperature under different cooling rates. The inset shows H_0 in the glassy state as a function of the cooling rate. The line is a guide for the eye.

As shown in Fig. 3, the glass transition also manifests itself by a break of slope within the temperature-dependence of the molar volume, although we note that the transition does not appear as sharp as in the case of the ground-state enthalpy. Nevertheless, our simulations reproduce the trend that is typically observed experimentally, i.e., the molar volume of the glass decreases with decreasing cooling rate (see the inset of Fig. 3). Note that an opposite trend is observed in glassy silica [4,8], that is, the molar volume of the glass increases with decreasing cooling rate. This is a consequence of the anomalous behavior of supercooled liquid silica, which features a minimum of molar volume (observed around 4800 K with the BKS potential [4,8]). In that respect, sodium silicate behaves in a more conventional way than silica and, as such, offers a better archetypical model to assess the general role of the cooling rate in controlling glass properties.

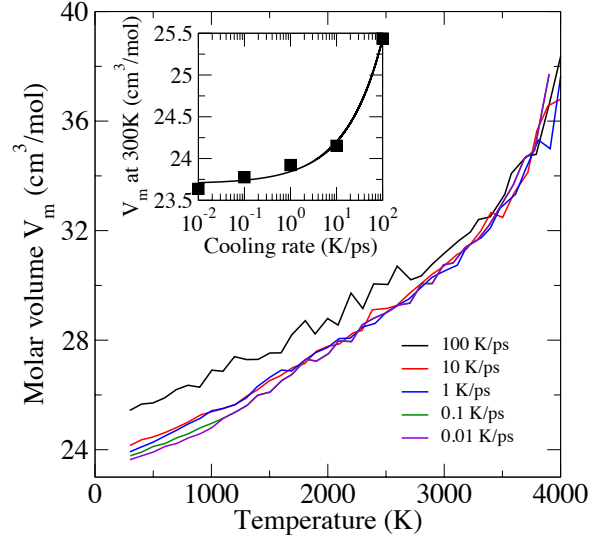


Fig. 3: Molar volume (V_m) as a function of temperature under different cooling rates. The inset shows V_m in the glassy state as a function of the cooling rate. The line is a guide for the eye.

A linear fit of low-temperature part of the molar volume curves from Fig. 3 yields the volumetric coefficient of thermal expansion (CTE) [37]. We note that our simulations overestimate the value of the CTE – the experimental data ranging between 3.6 and $3.9 \cdot 10^{-5} \text{ K}^{-1}$) [38,39]. Overall, we do not observe significant variations in the CTE for varying cooling rates. As shown in Fig. 3, this behavior strongly differs from the trend observed for glassy silica [8], wherein the CTE drops toward zero as the cooling rate decreases. In contrast, the present data suggest that the CTE of sodium silicate only slightly decreases toward the experimental value at low cooling rate. This different behavior can be understood from the fact that, in contrast to silica, sodium silicate continues to relax even below the fictive temperature (see the continuous decrease of energy in Fig. 2). Such low temperature relaxation appears to reduce the influence of the cooling rate on the thermal expansion of the glass.

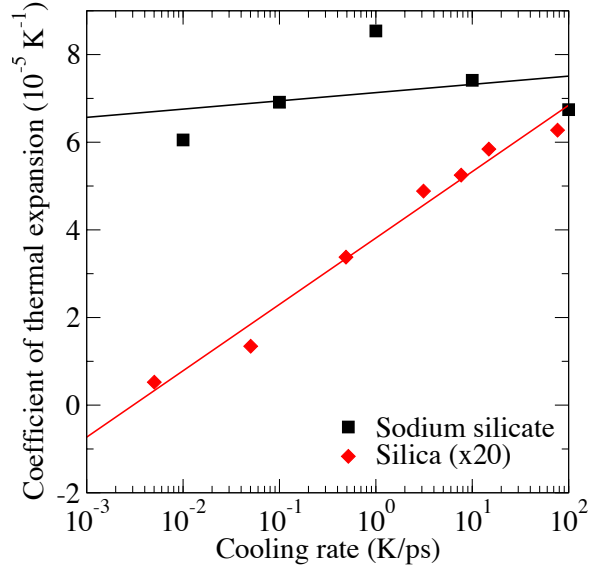


Fig. 4: Computed coefficients of thermal expansion of sodium silicate glasses as a function of the cooling rate. The data are compared to those obtained for glassy silica [8] (multiplied by a factor of 20 to facilitate comparison). The lines serve as guides for the eye.

2. Short-range order structure

a. Pair distribution function

We now focus our attention to the short-range order ($< 3 \text{ \AA}$) structure of the formed glasses. Fig. 5 shows the Si–O and Na–O partial pair distribution functions (PDFs). No significant shift is observed within the first and second coordination shell peaks. This suggests that the cooling rate does not significantly affect the local environment (bond distance, coordination number) of Si and Na cations. This contrasts with the results obtained for glassy silica, wherein the Si–O PDF featured some significant variation with respect to the cooling rate [4]. On the other hand, as shown in Fig. 6, the Si–Si and Na–Na PDFs exhibit a more pronounced dependence on the cooling rate. First, we observe that, for both PDFs, the first peak becomes sharper upon slower cooling rate. This denotes the formation of a more ordered atomic network. Second, we note that the first peak of the Si–Si PDF shifts toward higher distance as the cooling rate decreases. Since this Si–O bond distance remains largely unaffected by the cooling rate (see Fig. 5a), this suggests that the Si–O–Si bond angle is increasing for lower cooling rates (see Sec. III.2.b). In contrast, we observe that the first peak of the Na–Na PDF shifts toward lower distance as the cooling rate decreases. This suggests that Na atoms tend to “cluster” together inside pockets with lower cooler rates, in agreement with the picture of Greaves’ modified random network model [24,40].

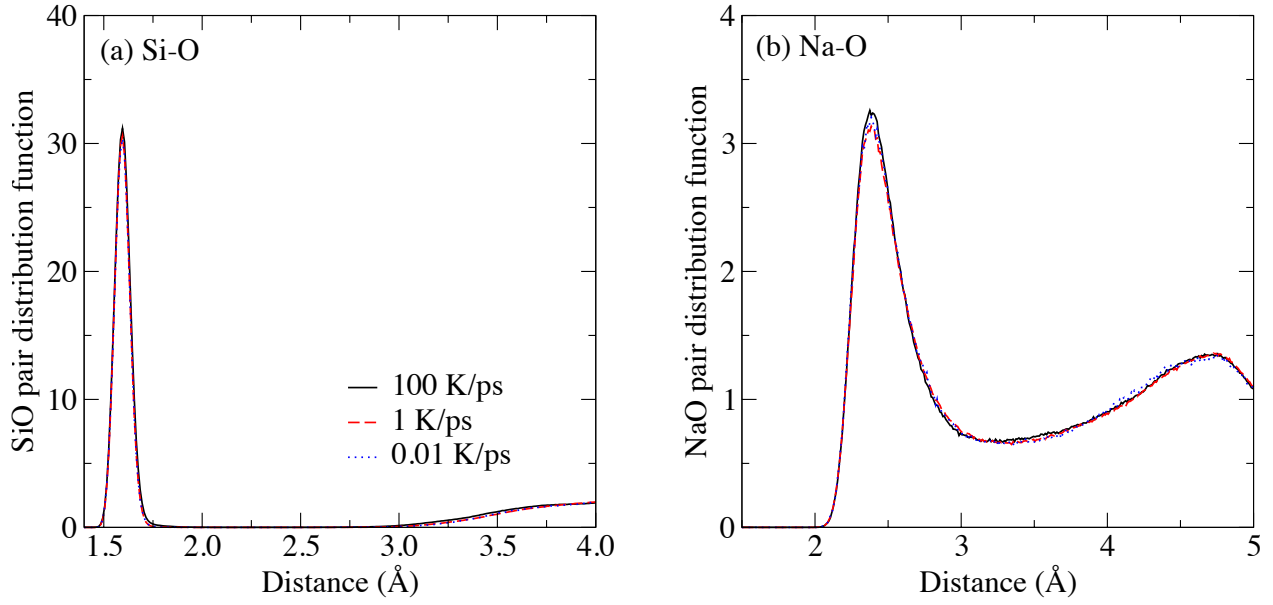


Fig. 5: (a) Si–O and (b) Na–O partial pair distribution functions in the glassy state for selected cooling rates.

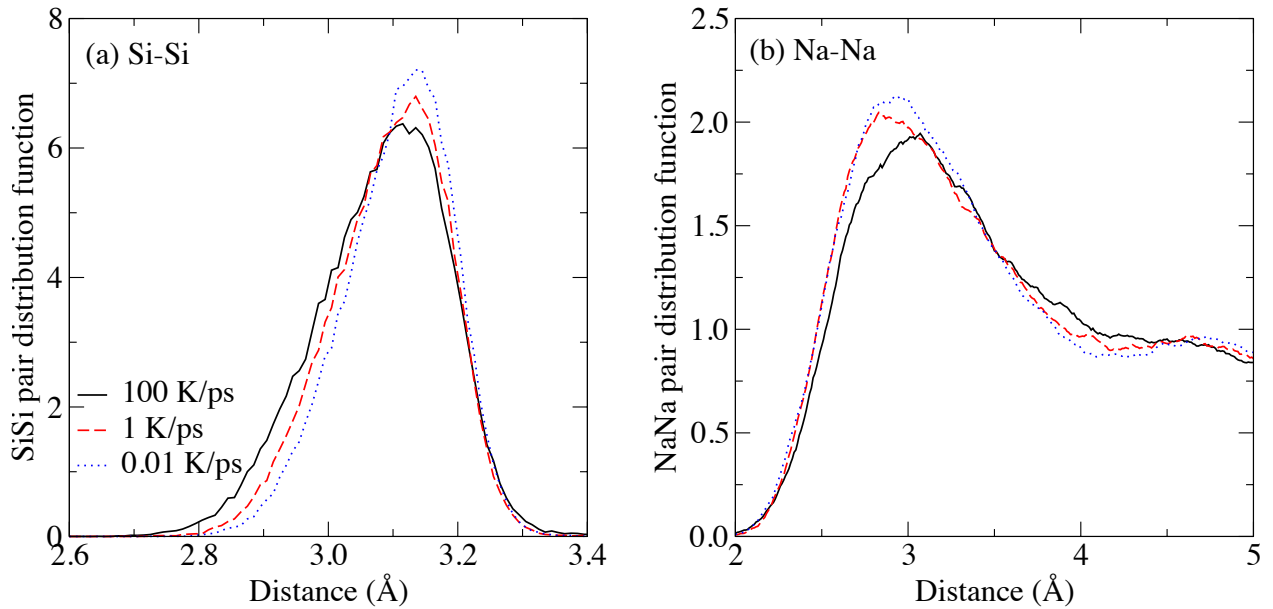


Fig. 6: (a) Si–Si and (b) Na–Na partial pair distribution functions in the glassy state for selected cooling rates.

b. Angles

The fact that the Si–Si PDF exhibits some dependence on the cooling rate although the Si–O one remains largely unaffected suggests that the cooling might have a more significant influence on angles than bond lengths. Fig. 7 shows the O–Si–O (intra-tetrahedral) and Si–O–Si (inter-

tetrahedral) bond angle distributions (BADs). First, we observe that both BADs becomes significantly sharper as the cooling rate decreases (see the insets of Fig. 7), which suggests that lower cooling rates result in higher angular order. Second, we note that the average value of the O–Si–O angle remains largely unaffected by the cooling rate, with a value that is close to 109° , as expected from the tetrahedral geometry of SiO_4 units. Similar conclusions were obtained in the case of glassy silica [8]. In contrast, we observe that the Si–O–Si BAD exhibits a significant shift toward higher angles as the cooling rate decreases. A similar behavior was observed in silica [4,8] and calcium aluminosilicate glasses [41,42], which suggests that this feature is general to silicate glasses. In the case of silica, the opening of the Si–O–Si was noted to indicate an opening of the network [4,8], in agreement with the decrease of the density as the cooling rate decreases. Here, this opening appears to be in contradiction with the observed increase of the density with lower cooling rates (see Fig. 3). This discrepancy might be explained by the fact that, in the case of sodium silicate, the opening of the Si–O–Si angle facilitates the formation of large pockets of Na. As such, although the opening of the inter-tetrahedral angle mostly results in the creation of some empty space in silica, network modifiers species like Na cations can fill these voids, which ultimately results in a more efficient overall atomic packing.

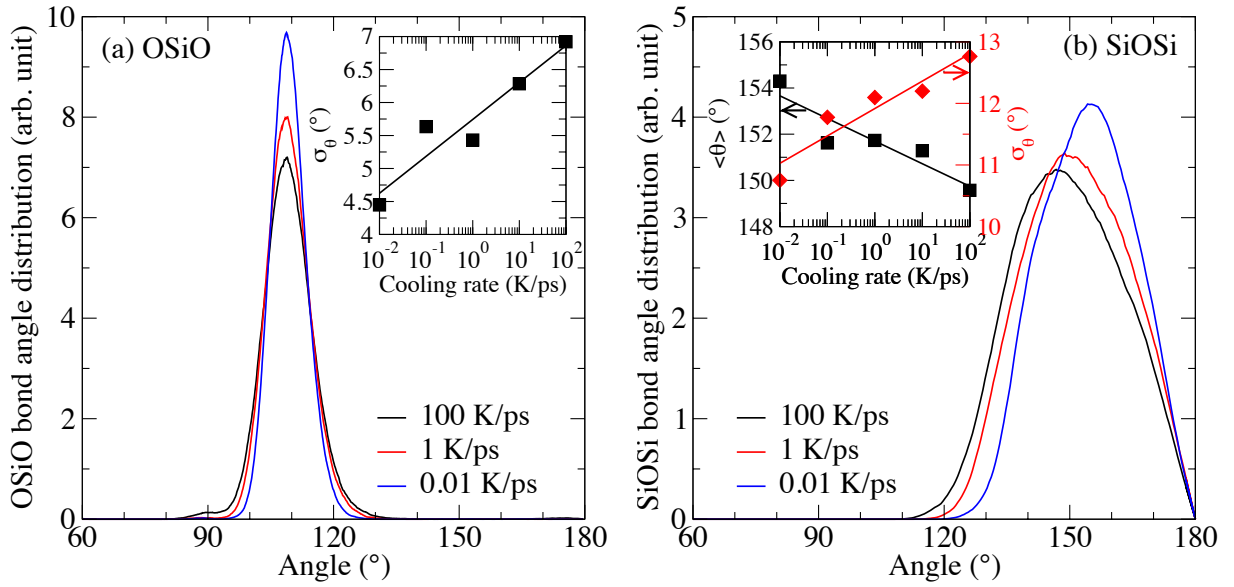


Fig. 7: (a) Intra-tetrahedral O–Si–O bond angle distribution (BAD) in the glassy state for selected cooling rates. The inset shows the standard deviation σ_θ of the BADs as a function of the cooling rate. The line is a guide for the eye. (b) Inter-tetrahedral Si–O–Si BAD in the glassy state for selected cooling rates. The inset shows the average value ($\langle\theta\rangle$, left axis) and standard deviation value (σ_θ , right axis) of the BADs as a function of the cooling rate. The lines serve as guides for the eye.

c. Connectivity

We now investigate the effect of the cooling rate on the connectivity of the atoms. As shown in Fig. 8, we observe the formation of a few ($< 1\%$) over-coordinated Si species at high cooling rate.

Similar observations were made in the case of glassy silica [4]. Such coordination defects are found to mostly disappear at lower cooling rates, although a small fraction of defects is still found. On the other hand, we observe that the coordination number of Na cations noticeably increases with lower cooling rates. This agrees with the observation that Na cations tend to form some clusters inside the large pockets created within the network following the opening of the Si–O–Si angle.

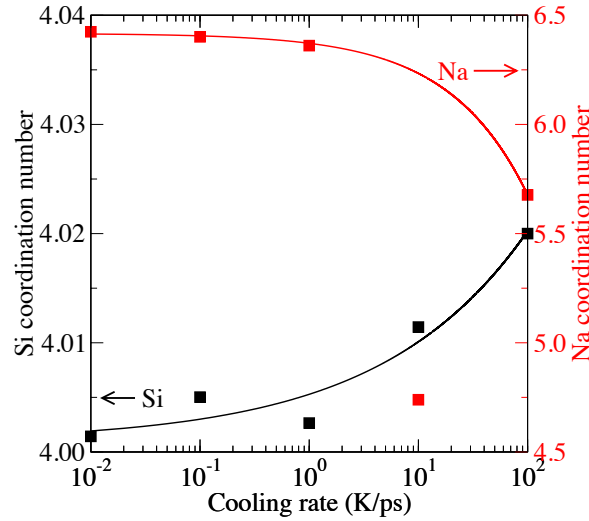


Fig. 8: Average coordination number of Si (left axis) and Na (right axis) atoms in the glassy state as a function of the cooling rate. The lines serve as guides for the eye.

We now focus on the O species. In glassy silica, the SiO_4 tetrahedra are connected to each other through their corners, so that the network only feature bridging oxygen (BO) species [6]. In contrast, Na cations tend to depolymerize the network by breaking Si–BO–Si bonds. Namely, each added Na cation results in the creation of a non-bridging oxygen (NBO) species through the formation of Si–O–Na bonds [6]. As shown in Fig. Fig. 9, we observe that the fraction of NBO increases as the cooling rate decreases and quickly plateaus toward the theoretical value at low cooling rate, i.e., assuming that the number of NBOs equals that of Na cations.

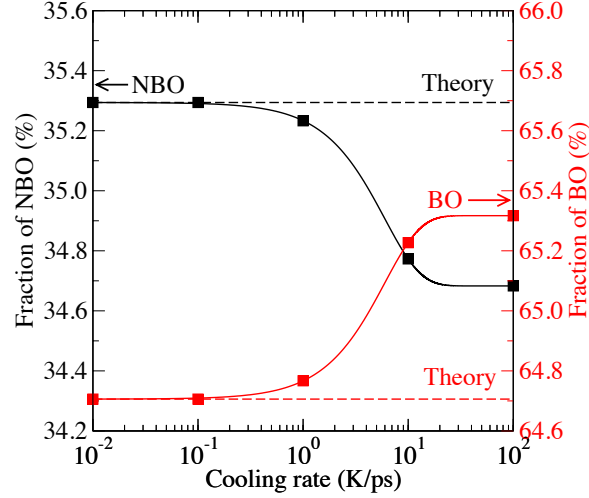


Fig. 9: Fraction of non-bridging (NBO, left axis) and bridging oxygen (BO, right axis) in the glassy state as a function of the cooling rate. The solid lines serve as guides for the eye. The dashed lines indicate the theoretical values, that is, assuming that each Na atom creates 1 NBO.

3. Medium-range order structure

We now turn our attention to the medium-range order structure ($3 < r < 10$ Å) of the sodium silicate glasses. We first focus on the connectivity around SiO_4 tetrahedra units, which can be assessed from the knowledge of the Q^n distribution, where a Q^n species denotes a SiO_4 tetrahedral unit connected to n other Si atoms, that is, comprising n BO atoms. Fig. 10 shows the fraction of the Q^n species as a function of the cooling rate. At high cooling rate, the distribution of the Q^n units is in close agreement with the prediction from a random model, wherein the NBO are randomly attributed to each Si atoms (see Ref. [19] for details). However, these results largely differ from experimental data [43], which present an excess of Q^3 units with respect to the predictions of the random model [19]. Interestingly, we observe that the fraction of Q^3 units increases with decreasing cooling rate, although it remains low as compared to the experimental value (around 68% [43]). This suggests that, as the cooling rate decreases, the atomic network self-organizes to favor the formation of Q^3 units through the transformation $Q^2 + Q^4 \rightarrow 2Q^3$ (see Sec. IV.1 for a discussion on this point).

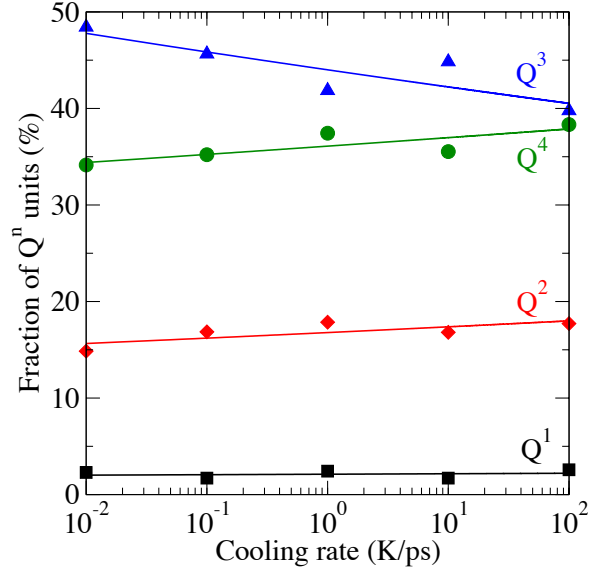


Fig. 10: Fraction of the Q^n species in the glassy state as a function of the cooling rate. The lines serve as guides for the eye.

Although they contain the same information as the partial PDFs, the partial structure factors place higher emphasis on structural correlations at higher distance and, hence, can also be used to assess the effect of the cooling rate on the medium-range order. As shown in Fig. 11, we observe that the partial structure factors are more affected by the cooling rate than the PDFs. In particular, the first-sharp diffraction peak (FSDP), which captures structural correlations within the medium-range order [23,44], exhibits significant variations in both its height and position with varying cooling rates. The FSDP of both the Si–Si and O–O partial structure factors is found to sharpen at lower cooling rate, which denotes an increased degree of order within the medium-range order of the atomic network. In both cases, we also observe a shift of the FSDP toward lower values of reciprocal wave vector, as observed in glassy silica [4]. This is in agreement with the opening of the silicate network resulting from the increase of the average inter-tetrahedral angle.

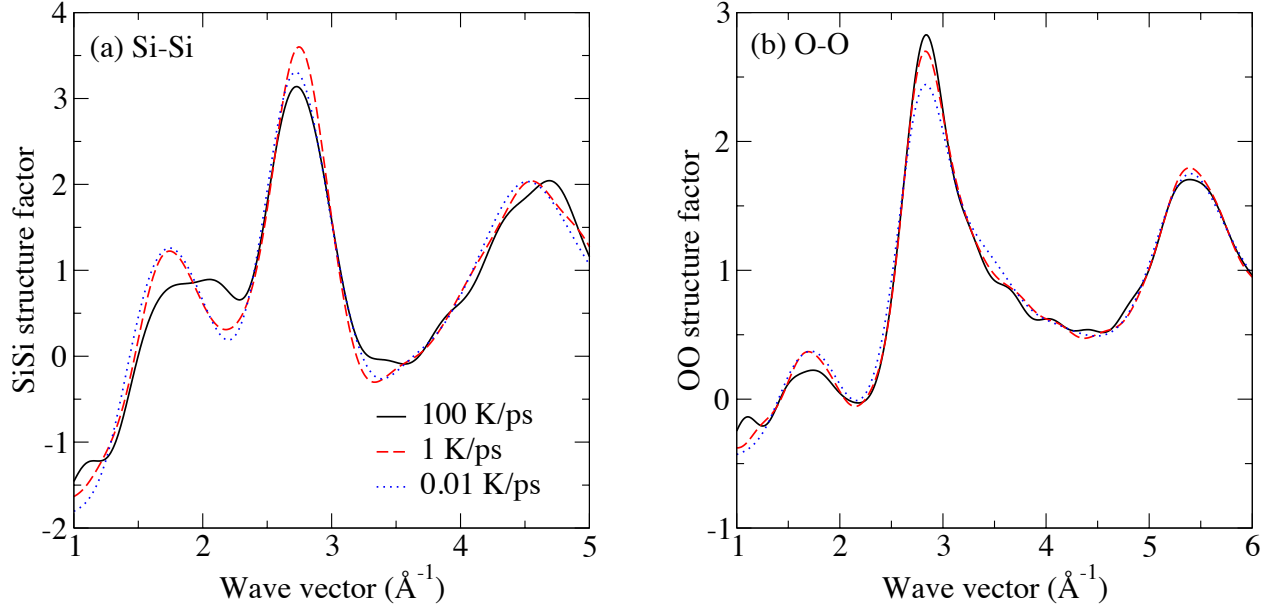


Fig. 11: (a) Si-Si and (b) O-O partial structure factors in the glassy state for selected cooling rates.

IV. Discussion

1. Linking MD simulations and experiments

We now discuss on how the predictions of the present MD simulations can be compared to experimental data despite the vast difference in the order of magnitude of the numerical and experimental cooling rates. To this end, we focus on the behaviors of the fictive temperature and Q^n distributions, as these properties are traditionally arguably challenging to be properly predicted by MD simulations.

Various functions have been proposed to describe the evolution of T_f as a function of the cooling rate (γ). In particular, a Vogel-Fulcher temperature-dependence of the viscosity (or relaxation time) yields the following form [4]:

$$T_f = T_0 - \frac{B}{\ln(\gamma A)} \quad \text{Eq. 1}$$

where T_0 is the fictive temperature infinitely small cooling rate, and A and B some parameters. Note that an Arrhenius behavior is obtained in the limit of $T_0 = 0$. Alternatively, mode-coupling theory [45] suggests a power law dependence as [4]:

$$T_f = T_0 + (A\gamma)^{1/\delta} \quad \text{Eq. 2}$$

where A and δ are some parameters.

Fig. 12 shows the evolution of the computed fictive temperature as a function of the cooling rate, as compared to the experimental value obtained at low cooling rate [46]. As expected and observed experimentally [6], T_f is found to decrease with decreasing cooling rate. The computed values of T_f were then fitted based on the functions mentioned below and extrapolated to lower cooling rates for comparison with the experimental data. Overall, we observe that the computed values are reasonably well fitted by Eq. 1 and Eq. 2. In contrast, the fits offered assuming an Arrhenius or logarithmic dependence are significantly less satisfactory. Similar results were observed in the case of glassy silica [4]. However, when extrapolated toward lower cooling rate for comparison with the experimental value of T_f (733 K [46]), we note that both the Vogel-Fulcher and mode-coupling theories significantly over-predict T_f , the fits using Eq. 1 and Eq. 2 yielding $T_0 = 1050$ and 1330 K, respectively. This is in agreement with the fact that the Vogel-Fulcher equation typically breaks down at low temperature [47]. On the other hand, the Arrhenius form offers an excellent extrapolation toward the experimental data. Note that this type of Arrhenius dependence is typically observed experimentally [6].

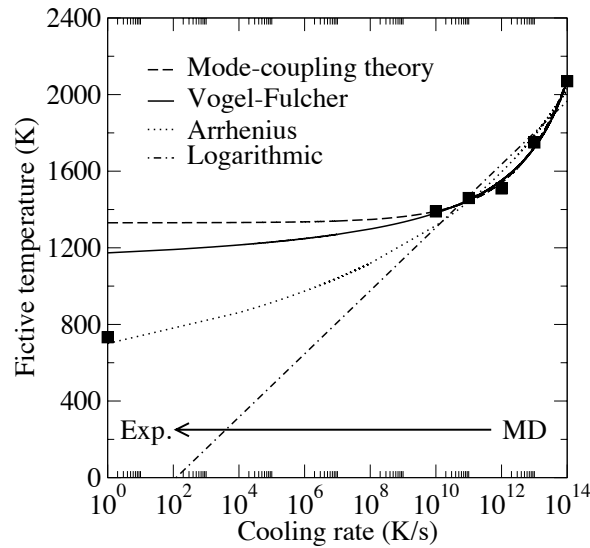


Fig. 12: Experimental [46] and computed fictive temperature (T_f) as a function of the cooling rate (γ). The computed data are fitted following the Vogel-Fulcher equation (Eq. 1, solid line), mode-coupling theory (Eq. 2, dashed line), the Arrhenius equation (dotted line), and a simple logarithmic law (dashed-dotted line). The obtained fits are extrapolated toward lower cooling rates for comparison with the experimental values.

Coming back to the structure of the glass, the Q^n distribution is arguably the structural feature of the silicate glasses that is the most challenging to predict for MD simulations, which usually yield values that closely follow the predictions from a random model [19]. Note that the usage of very large systems did not offer any significant improvements in this matter [48]. Fig. 13 shows the fraction of each Q^n species as a function of the cooling rate. We note that the computed data can be well fitted by a simple logarithmic function. This type of dependence can be predicted by

considering the cooling process as an optimization problem [4,49]. When extrapolated toward lower cooling rate, we observe that the logarithmic fits favorably compare with experimental values. A power law fit (not shown here) also yields a good agreement with the experimental data. Overall, these results suggest that, although MD simulations are intrinsically limited to high cooling rate due to the high computational cost, their outcomes can be directly compared to those obtained with more realistic cooling rates by extrapolation.

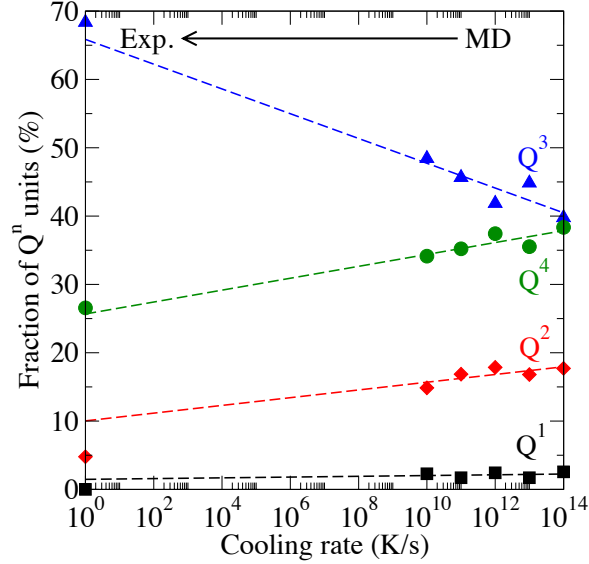


Fig. 13: Experimental [43] and computed fractions of the Q^n species in the glassy state as a function of the cooling rate. The computed fractions are fitted assuming a logarithmic law and extrapolated toward lower cooling rates for comparison with the experimental values

2. Decoupling of enthalpy and volume relaxation

Finally, we assess whether the evolutions of the more enthalpy and volume upon varying cooling rates are coupled to each other. To this end, we first fitted the data by a power law, as suggested by mode-coupling theory [45]:

$$Y(\gamma) = Y_0 + (A\gamma)^\delta \quad \text{Eq. 3}$$

where $Y(\gamma)$ refers to the molar enthalpy or volume and Y_0 its limit value for an infinitely small cooling rate. We then define a normalized “relaxation function” $f(\gamma)$ as:

$$f(\gamma) = \frac{Y(\gamma) - Y_0}{(A\gamma_{\max})^\delta} = \left(\frac{\gamma}{\gamma_{\max}} \right)^\delta \quad \text{Eq. 4}$$

where $\gamma_{\max} = 10^{14}$ K/s. By definition, $f(0) = 0$ and $f(\gamma_{\max}) = 1$. The shape of the relaxation function is then captured by the exponent δ , where a small value of δ indicates that the property

slowly relaxes toward its limit value as the cooling rate decreases, whereas a large value of δ indicates that the property quickly relaxes toward its limit value.

Fig. 14 shows the relaxation function of the molar enthalpy and volume. Interestingly, we observe a clear decoupling between the relaxation of these two quantities, namely, the enthalpy ($\delta = 0.43$) converges toward its limit value much faster than the molar volume ($\delta = 0.12$). Such decoupling was also observed in the cases of the room-temperature relaxation of a silicate glass [34,50] and the response to irradiation of quartz [51,52]. Based on the results above, this decoupling can be understood as follows. On one hand, the enthalpy mostly depends on the short-range order of each atom (bond length, coordination number, angles) as the interaction energy between atoms and their second coordination shell is significantly lower. Based on the results above, we observe that the short-range order structure of sodium silicate quickly plateaus as the cooling rate decreases. This arises from the fact short-range order reorganizations do not involve any collective motion of atoms and, as such, are associated to low relaxation times. In turn, short-range defects are associated to a significant energy penalty. Altogether, the relaxation of the short-range order (and hence, of the enthalpy) is favored by kinetics and thermodynamics. In contrast, the volume depends on the short-range order, but also on the medium-range order (FSDP, Q^n distribution, rings, etc.). We observe that the medium-range order structural features of the glass show a greater dependence to the cooling rate. This arises from the fast the relaxation of such features requires some collective reorganizations of atoms and, as such, are associated to longer relaxation times. In turn, since the medium-range order contribution to the energy of the system is low, there is no significant driving force for such relaxation. Hence, the relaxation of the medium-range order (and hence, of the volume) is not thermodynamically favored and exhibits a slow kinetics.

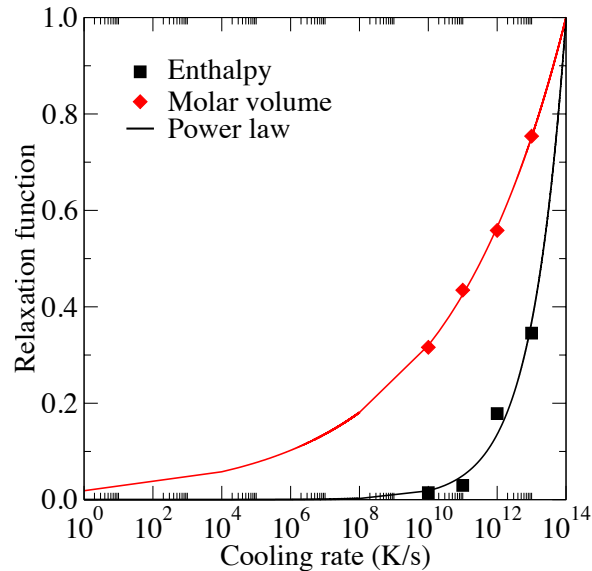


Fig. 14: Relaxation function (see text) of the enthalpy and molar volume as a function of the cooling rate. The data are fitted by a power law.

V. Conclusion

Overall, the cooling rate is found to affect the structure and properties of sodium silicate glass. However, we find that the short-range order structure (bond lengths, coordination numbers, and angles) of the glass only weakly depends on the cooling rate, whereas the medium order appears to be more affected. This results in a decoupling between the relaxation of the enthalpy and volume with decreasing cooling rates. Further, despite the intrinsic limitation of MD simulations to the usage of high cooling rate, our simulations show that a handshake between experiments and MD simulations can be achieved by extrapolating the outcomes of the simulations toward lower cooling rates.

Acknowledgements

This work was supported by the National Science Foundation under Grant No. 1562066 and Corning Incorporated.

References

- [1] J. Du, in *Mol. Dyn. Simul. Disord. Mater.*, edited by C. Massobrio, J. Du, M. Bernasconi, and P. S. Salmon (Springer International Publishing, 2015), pp. 157–180.
- [2] A. Pedone, G. Malavasi, A. N. Cormack, U. Segre, and M. C. Menziani, *Theor. Chem. Acc.* **120**, 557 (2008).
- [3] X. Yuan and A. N. Cormack, *J. Non-Cryst. Solids* **283**, 69 (2001).
- [4] K. Vollmayr, W. Kob, and K. Binder, *Phys. Rev. B* **54**, 15808 (1996).
- [5] P. Y. Huang, S. Kurasch, J. S. Alden, A. Shekhawat, A. A. Alemi, P. L. McEuen, J. P. Sethna, U. Kaiser, and D. A. Muller, *Science* **342**, 224 (2013).
- [6] A. K. Varshneya, *Fundamentals of Inorganic Glasses* (Academic Press Inc, 1993).
- [7] K. Vollmayr, W. Kob, and K. Binder, *J. Chem. Phys.* (1998).
- [8] J. M. D. Lane, *Phys. Rev. E* **92**, 12320 (2015).
- [9] G. Agnello and A. N. Cormack, *J. Non-Cryst. Solids* **451**, 146 (2016).
- [10] Y. Yu, B. Wang, M. Wang, G. Sant, and M. Bauchy, *J. Non-Cryst. Solids* **443**, 148 (2016).
- [11] C. A. Angell, *J. Non-Cryst. Solids* **131**, 13 (1991).
- [12] J. C. Mauro, *Frontiers Mater.* **1**, 20 (2014).
- [13] J. C. Mauro and E. D. Zanotto, *Int. J. Appl. Glass Sci.* **5**, 313 (2014).
- [14] J. C. Mauro, C. S. Philip, D. J. Vaughn, and M. S. Pambianchi, *Int. J. Appl. Glass Sci.* **5**, 2 (2014).
- [15] J. C. Mauro, A. J. Ellison, and L. D. Pye, *Int. J. Appl. Glass Sci.* **4**, 64 (2013).
- [16] M. Bauchy, B. Guillot, M. Micoulaut, and N. Sator, *Chem. Geol.* **346**, 47 (2013).
- [17] J. Du and A. Cormack, *J. Non-Cryst. Solids* **349**, 66 (2004).
- [18] A. N. Cormack, J. Du, and T. R. Zeitler, *Phys Chem Chem Phys* **4**, 3193 (2002).
- [19] M. Bauchy, *J. Chem. Phys.* **137**, 44510 (2012).
- [20] S. Plimpton, *J. Comput. Phys.* **117**, 1 (1995).
- [21] J. Du and L. R. Corrales, *Phys. Rev. B* **72**, 92201 (2005).

- [22] J. Du and L. R. Corrales, *J. Non-Cryst. Solids* **352**, 3255 (2006).
- [23] M. Micoulaut and M. Bauchy, *Phys. Status Solidi B* **250**, 976 (2013).
- [24] M. Bauchy and M. Micoulaut, *Phys. Rev. B* **83**, 184118 (2011).
- [25] M. Bauchy and M. Micoulaut, *Phys. Rev. Lett.* **110**, 95501 (2013).
- [26] M. Bauchy and M. Micoulaut, *Nat. Commun.* **6**, 6398 (2015).
- [27] B. Mantsi, M. Bauchy, and M. Micoulaut, *Phys. Rev. B* **92**, 134201 (2015).
- [28] M. Bauchy, B. Wang, M. Wang, Y. Yu, M. J. Abdolhosseini Qomi, M. M. Smedskjaer, C. Bichara, F.-J. Ulm, and R. Pellenq, *Acta Mater.* **121**, 234 (2016).
- [29] B. Wang, Y. Yu, Y. J. Lee, and M. Bauchy, *Front. Mater.* **2**, 11 (2015).
- [30] B. Wang, Y. Yu, M. Wang, J. C. Mauro, and M. Bauchy, *Phys. Rev. B* **93**, 64202 (2016).
- [31] A. Pedone, G. Malavasi, A. N. Cormack, U. Segre, and M. C. Menziani, *Chem. Mater.* **19**, 3144 (2007).
- [32] A. C. Wright, A. G. Clare, B. Bachra, R. N. Sinclair, A. C. Hannon, and B. Vessal, *Trans Am Crystallogr Assoc* **27**, 239 (1991).
- [33] A. C. Wright, *J. Non-Cryst. Solids* **159**, 264 (1993).
- [34] Y. Yu, M. Wang, D. Zhang, B. Wang, G. Sant, and M. Bauchy, *Phys. Rev. Lett.* **115**, 165901 (2015).
- [35] B. Ruta, G. Baldi, Y. Chushkin, B. Rufflé, L. Cristofolini, A. Fontana, M. Zanatta, and F. Nazzani, *Nat. Commun.* **5**, (2014).
- [36] P. G. Debenedetti and F. H. Stillinger, *Nature* **410**, 259 (2001).
- [37] M. Wang, B. Wang, N. M. A. Krishnan, Y. Yu, M. M. Smedskjaer, J. C. Mauro, G. Sant, and M. Bauchy, *J. Non-Cryst. Solids* **455**, 70 (2017).
- [38] H. F. Shermer, *J. Res. Natl. Bur. Stand.* **57**, (1956).
- [39] G. K. White, J. A. Birch, and M. H. Manghnani, *J. Non-Cryst. Solids* **23**, 99 (1977).
- [40] B. Vessal, G. N. Greaves, P. T. Marten, A. V. Chadwick, R. Mole, and S. Houde-Walter, *Nature* **356**, 504 (1992).
- [41] M. M. Smedskjaer, M. Bauchy, J. C. Mauro, S. J. Rzoska, and M. Bockowski, *J. Chem. Phys.* **143**, 164505 (2015).
- [42] M. Wang, B. Wang, T. K. Bechgaard, J. C. Mauro, S. J. Rzoska, M. Bockowski, M. M. Smedskjaer, and M. Bauchy, *J. Non-Cryst. Solids* **454**, 46 (2016).
- [43] H. Maekawa, T. Maekawa, K. Kawamura, and T. Yokokawa, *J. Non-Cryst. Solids* **127**, 53 (1991).
- [44] S. R. Elliott, *J. Non-Cryst. Solids* **182**, 40 (1995).
- [45] W. Kob and H. C. Andersen, *Phys. Rev. E* **51**, 4626 (1995).
- [46] Y. Vaills, T. Qu, M. Micoulaut, F. Chaimbault, and P. Boolchand, *J. Phys.-Condens. Matter* **17**, 4889 (2005).
- [47] J. C. Mauro, Y. Yue, A. J. Ellison, P. K. Gupta, and D. C. Allan, *Proc. Natl. Acad. Sci.* **106**, 19780 (2009).
- [48] L. Adkins and A. Cormack, *J. Non-Cryst. Solids* **357**, 2538 (2011).
- [49] D. A. Huse and D. S. Fisher, *Phys. Rev. Lett.* **57**, 2203 (1986).
- [50] Y. Yu, J. C. Mauro, and M. Bauchy, *Am. Ceram. Soc. Bull.* **96**, 34 (2017).
- [51] B. Wang, N. M. A. Krishnan, Y. Yu, M. Wang, Y. Le Pape, G. Sant, and M. Bauchy, *J. Non-Cryst. Solids* **463**, 25 (2017).

[52] B. Wang, Y. Yu, I. Pignatelli, G. Sant, and M. Bauchy, J. Chem. Phys. **143**, 24505 (2015).